

# Extraction of a deterministic component from ROSAT X-ray data using a wavelet transform and the principal component analysis

L. Liszka<sup>1,\*</sup> and M. Holmström<sup>2</sup>

<sup>1</sup> Steward Observatory, University of Arizona, Tucson, AZ, U.S.A.

<sup>2</sup> Swedish Institute of Space Physics, S-981 28 Kiruna, Sweden

Received April 23; accepted August 23, 1999

**Abstract.** In the present work wavelet transform methods together with principal component analysis and non-linear filtering are used to extract the deterministic components in AGN X-ray variability from the photon event history files. The photon history files are converted into so called ampligrams using the Morlet wavelet transform. The ampligram may be considered as an analogy to signal decomposition into Fourier components. In that case different components correspond to different frequencies. In the present case different components correspond to different wavelet coefficient magnitudes, being equivalent to spectral densities. In addition to the ampligram a time scale spectrum is defined, being a forward wavelet transform of each row (wavelet coefficient magnitude) in the ampligram. The time scale spectrum of the ampligram tells us more than the original wavelet spectrum does. The time scale spectrum reveals individual signal components and indicates the statistical properties of each component: deterministic or stochastic. The ampligram and its time scale spectrum seems to be a useful tool to study processes resulting in a mixture of stochastic and deterministic components. In the case of X-ray luminosity variations in the AGN it is expected that the described data analysis technique will provide a conclusive proof of the existence of building blocks. The efficient decomposition of the luminosity variation data may be used to study the deterministic, quasi-periodic phenomena, like tones and chirps. The most important point of the method is that it may be used to remove the influence of the Poisson statistics in the photon data and in this way to extract real deterministic luminosity variations. As it is shown by simulations in the final part of this work, the method is capable to extract weak, of the order of few percent, deterministic variations embedded in a totally Poisson-like series of events. There may be

also other applications of the method in astrophysics, for example to study X-ray pulsars.

**Key words:** methods: data analysis — pulsars: individual 1E2259+586 — galaxies: individual NGC 4051; NGC 5548 — galaxies: Seyfert — X-rays: galaxies

## 1. Introduction

There is some evidence that X-ray photons from astronomical sources can not be fully described by a Poisson process. There seems to be a deterministic modulation of the photon series which is reflected in observed wavelet spectra of photon counts. The following experiment may be performed using the photon event data in order to test the above statement: Let us select 5 consecutive photon events observed at instants:  $t_1$ ,  $t_2$ ,  $t_3$ ,  $t_4$  and  $t_5$ . Let us assume that the occurrence of a photon at  $t_3$  is conditioned by occurrences at preceding instants  $t_1$ ,  $t_2$  and following instants  $t_4$  and  $t_5$ . Using a large population of sets of 5 consecutive photons it is possible to create a statistical model of the photon train using, for example, the neural network technique. That technique, being a kind of a non-linear interpolation, has been used to reconstruct uniformly sampled data, even when many data points were missing in an observed chaotic process (Liszka 1996).

If the photon data would follow a true Poisson process, it would be impossible to create such a model. However, it has been found, that even a simplest model consisting of a single back-propagation network, could be trained with rms errors usually less than 30%. This means that the conditional probability of a photon event at  $t_3$ , conditioned by photon events at  $t_1$ ,  $t_2$ ,  $t_4$  and  $t_5$ :

$$P(t_3|t_1, t_2, t_4, t_5) > 0. \quad (1)$$

Send offprint requests to: L. Liszka, e-mail: ludwik@irf.se

\* Permanent address: Swedish Institute of Space Physics, Umeå Division, Sörfors 634, S-905 88 Umeå, Sweden.

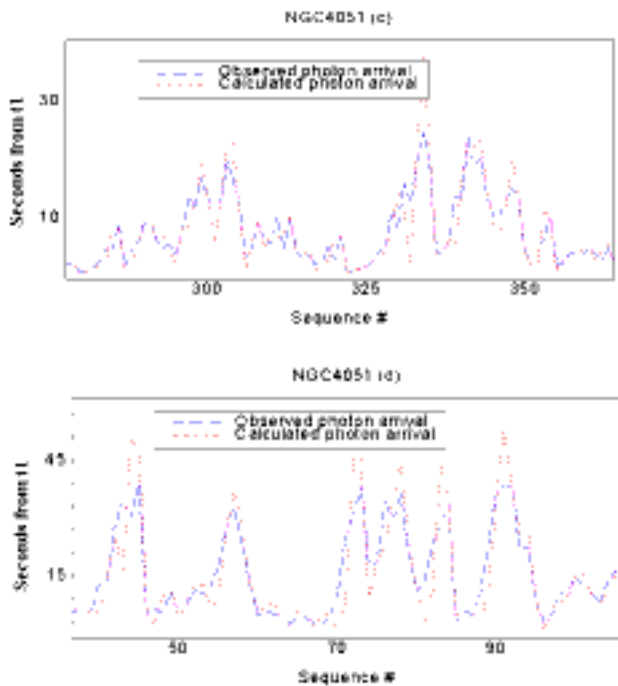


**Fig. 1.** Two examples of prediction of photon events at  $t_3$  for photon data from NGC 4051 observed by the ROSAT satellite.  $t_3$  is expressed in seconds counted from  $t_1$

The above fact is an indication that the photon events do not follow a Poisson process. In a true Poisson process it would be impossible to predict the occurrence of an event at  $t_3$ . Two examples of prediction of photon events at  $t_3$  for photon data from NGC 4051 observed by the ROSAT satellite are shown in Fig. 1. A single back-propagation neural network with 9 processing elements in the hidden layer has been used to construct a model of the photon series. Using a more complex model of hybrid type (Liszka 1996) it would be possible to obtain even better prediction accuracy (cf. Fig. 1).

Another proof for deterministic variations of the photon series is the fact that if the image is divided into two or four equal parts, variations of photon counts in individual parts are correlated. An example of photon-count variations in NGC 5548 recorded by the ROSAT satellite (ROR 701242) in two halves of the image is shown in Fig. 2.

However, it would also be the case if variations would be imposed by the measuring instrument. In such case the short time variations of different sources in the same image would be correlated. This type of correlation has not been found, see an example in Fig. 3.

The conclusion of the above experiments is that the short-term variations of photon counts recorded by the satellite contain deterministic information, most likely corresponding to intensity variations of the source itself.

In the case of X-rays from AGN there is probably a physical source of deterministic variations of the photon

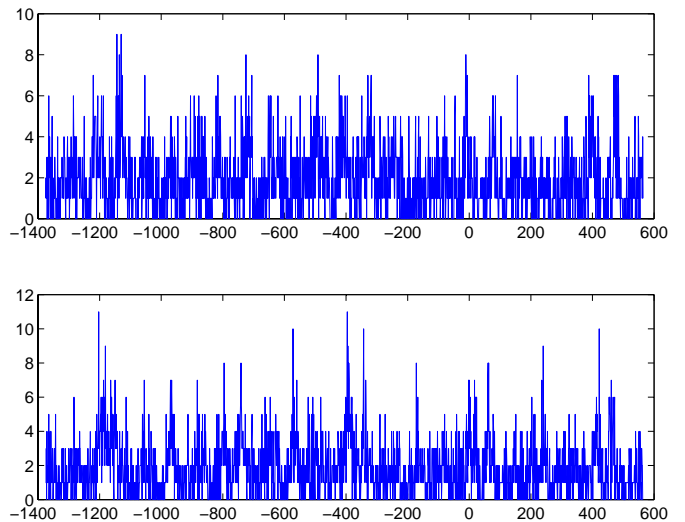


**Fig. 2.** An example of photon-count variations in NGC 5548 (ROR 701242) in two halves of the image. Photon energies  $< 0.5$  keV, 2 second sampling bins

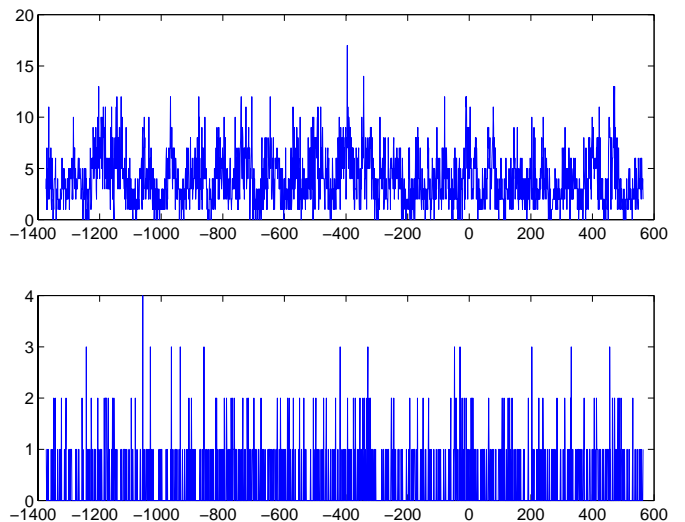


**Fig. 3.** An example of photon-count variations in NGC 5548 (ROR 701242) (upper graph) together with simultaneous variations of another source in the same image

flux. It seems that there are individual physical luminosity producing events in the AGN source itself which together constitute the X-ray light curve. There are two proposals for the nature of these elementary events. Pacholczyk & Stoeger (1994) propose “building blocks” in the X-ray photon flux from active galactic nuclei resulting from ballistic events due to smaller black holes passing through the accretion disk of the largest black hole in the cluster. Another proposal about the nature of these events is that they may be magnetohydrodynamic flares in the accretion disk around a single supermassive black hole (De Vries & Kuijpers 1992).

In the present study we discuss methods to extract the deterministic component from the photon event

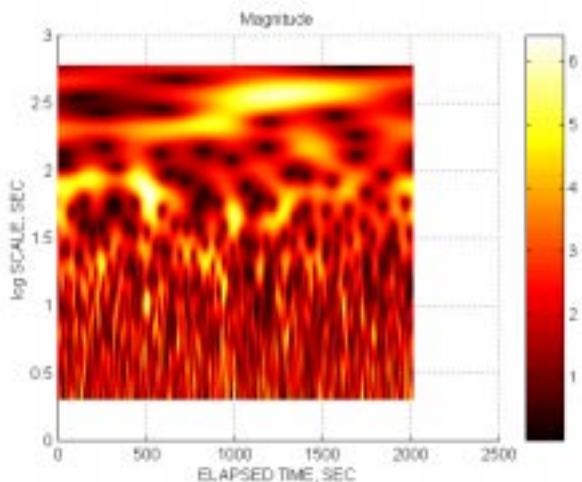


**Fig. 4.** The wavelet scalogram for NGC 5548 (ROR 701246), photon energies  $> 0.5$  keV. The vertical axis shows logarithm of time scales in s

histories. These methods are described in the remainder of the paper. It will be shown that wavelet spectra seem to be a useful tool to study the short-term temporal variations in the photon counting rate, even in cases of very low counting rates. Here we shall employ wavelet transform methods together with principal component analysis and nonlinear filtering to extract the deterministic components in AGN X-ray variability. The methods may be useful for understanding the dynamics of X-ray photon-count fluctuation. In the present paper the data analysis will be illustrated using a photon event history file from NGC 5548 (ROR 701246) and from the X-ray pulsar 1E2259+586 (ROR 400314), both for photon energies  $> 0.5$  keV. The wavelet scalogram for NGC 5548 (ROR 701246) is shown in Fig. 4.

## 2. Wavelet transform

The wavelet transform has become a powerful tool for frequency analysis, in particular for non-stationary time series. Discussions of the wavelet transform and its applications can be found in a number of recent books and review articles (Daubechies 1992; Chui et al. 1994; Farge 1992). The wavelet transform of a function  $y(t)$  is defined as (here  $*$  denotes complex conjugate):

$$w(a, b) = a^{-\frac{1}{2}} \int_{-\infty}^{+\infty} y(t) g^* \left( \frac{t-b}{a} \right) dt \quad (2)$$

where variable  $a$  is the scale dilation parameter and  $b$  the translation parameter. Both parameters are dimensionless. The real- or complex-valued function  $g(t)$  is called a mother (or analyzing) wavelet. Here a particular wavelet transform, the Morlet wavelet, will be used. The Morlet wavelet, being a locally periodic wave-train, is related to

windowed Fourier analysis. It is obtained by taking a complex sine wave, and by localizing it with a Gaussian (bell-shaped) envelope. The Morlet wavelet is defined as:

$$g(t) = \exp \left( i\omega_0 t - \frac{t^2}{2} \right) \quad (3)$$

and its Fourier transform:

$$G(\omega) = \sqrt{2\pi} \exp \left[ -\frac{(\omega - \omega_0)^2}{2} \right]. \quad (4)$$

The Morlet wavelet gives the smallest time-bandwidth product (Lagoutte et al. 1992).  $\omega_0$  is a phase constant (in the present study  $\omega_0 = 5$ ). For large  $\omega_0$  the frequency resolution improves, though at the expense of decreased time resolution. The dilation parameter may be considered as equivalent to the frequency of the analyzed signal, while the translation parameter corresponds to the time elapsed along the analyzed sample. In practice, for analyzing a discrete-time signal  $y(t_i)$  we sample the continuous wavelet transform on a grid in the time-scale plane  $(b, a)$  by choosing  $a = j$  and  $b = k$  where  $j$  and  $k$  are integers. That is we compute wavelet coefficients

$$w_{j,k} = j^{-1/2} \int_{-\infty}^{\infty} y(t) g^* \left( \frac{t-k}{j} \right) dt \quad (5)$$

where  $1 \leq j \leq J$  and  $1 \leq k \leq N$ . The integral in (5) is approximated using the discrete-time signal  $y(t_i)$ .

Since the wavelet transform is an over-complete representation of the original signal (a one-dimensional signal is transformed to the two-dimensional plane) there are many possibilities for reconstructing the signal. One way is to use a discrete version of Morlet's formula

$$y(b) = c \int_{-\infty}^{\infty} w(a, b) \frac{da}{a^{3/2}}. \quad (6)$$

Note that the original signal's low-pass (DC) component is lost in the transform.

In the present study dilation number 1 corresponds to the highest frequency (a half of sampling rate). The highest dilation number corresponds to the lowest observable frequency.

## 3. Time-series decomposition using wavelet transform

Many time series observed in physics consist of a deterministic part with a superimposed stochastic component. A powerful technique to separate both components has been proposed by Farge & Philipovitch (1993) and implemented in a practically usable software by Wernik & Grzesiak (1997). In that method, being a kind of non-linear filtering, called also the threshold filtering, a wavelet frequency spectrum of the time series is calculated. The time series is decomposed into two parts in the following

way:

- A deterministic “strong” part is obtained by setting to zero all wavelet coefficients less than a certain threshold level. The inverse wavelet transform is used to calculate the corresponding time series.
- A stochastic “weak” part is obtained by setting to zero all wavelet coefficients greater than that threshold level. The inverse wavelet transform is also used here to calculate the corresponding time series.
- New wavelet spectra are calculated for each partial time series.

Signal discrimination using the magnitude of wavelet coefficients as a discrimination criterion would correspond to discrimination with respect to the spectral density when using the Fourier transform. The stochastic part must follow a Gaussian probability distribution function. As a measure of departure from a Gaussian distribution the kurtosis is used. If the threshold is properly selected, the integral of the kurtosis of the stochastic part over the entire frequency range reaches a minimum.

In the present problem the method will be applied in the opposite manner. In the case of a photon train, reaching the measuring instrument at a low rate, there will be a dominating Poisson statistics modulated with a weak deterministic component. A low threshold will then be used to separate a weak, deterministic component from a strong, Poisson component.

#### 4. The ampligram

There is a straightforward generalization of the above technique, which may be used to separate independent components of the signal, assuming that the different components are characterized by different wavelet coefficient magnitudes (spectral densities). The experience from studies of oscillations in complex mechanical systems indicate that a given oscillation mode usually occurs with a certain amplitude/spectral density. The amplitude ratios between possible modes are usually constant in such a system. That observation may be used to generalize the above non-linear filtering technique. For a discrete-time signal  $y(t_i)$  the following operations are performed

1. Wavelet transform  $y(t_i)$ . This results in a complex  $J \times N$  matrix  $W = \{w_{j,k}\}$ .
2. Instead of using the low-pass or high-pass filtering of wavelet coefficient magnitudes, as described in Sect. 3, a kind of band-pass filtering of wavelet coefficient magnitudes is used.

Find the maximum magnitude among the wavelet coefficients,

$$|W| = \max_{j,k} |w_{j,k}|.$$

Define  $L$  magnitude intervals

$$I_l = [(l-1)\Delta w, l\Delta w], \quad l = 1, 2, \dots, L \quad (7)$$

with  $\Delta w = |W|/L$ .

Construct  $L$  matrices  $W_l$ ,  $l = 1, 2, \dots, L$ , such that

$$[W_l]_{j,k} = \begin{cases} w_{j,k} & \text{if } |w_{j,k}| \in I_l, \\ 0 & \text{otherwise.} \end{cases}$$

3. Inverse wavelet transform  $W_l$  to get new time-signals  $y_l(t_i)$ ,  $l = 1, 2, \dots, L$ . Each  $y_l(t_i)$  is what the signal would look like if only a narrow range of wavelet coefficient amplitude would be present in the signal.
4. Construct an  $L \times N$  matrix  $Y$  with  $y_l(t_i)$  as rows. This matrix  $Y$  is the *ampligram* of the original time-signal  $y(t_i)$ .

Note that if we just want to examine a subset of wavelet coefficient magnitudes, the construction of the intervals  $I_l$  in the above algorithm can be changed, e.g., choosing  $\Delta w = 0.2|W|/L$  results in a “low-20” ampligram.

An interesting application of the method is to study variability of a X-ray pulsar, even using data with low counting rate. Here, an ampligram of a 1024 seconds sample from 1E2259+586 taken by ROSAT PSPC instrument (file number ROR 400314), is shown in Fig. 6. That pulsar has been extensively studied (Parmar et al. 1998) by means of the BeppoSAX satellite. According to the above reference, the 0.5 – 10 keV pulse shape is characterized by a double peaked profile, with the amplitude of the second peak about 50% of that of the main peak. At the time when the analyzed ROSAT file was taken, the pulse period was about 6.97885 seconds (cf. Fig. 5 of Parmar et al. 1998). In order to construct the ampligram, photons were counted in 0.24 s bins. The bandwidth of 4% in the wavelet coefficient magnitude domain was used. The 4% band was moved in 1% steps over the range 0 – 20% of the maximum wavelet coefficient magnitude. It may be seen that 7 s pulses cover the range of wavelet coefficient magnitude between 5 and 14%. The ampligram reveals a semi-regular pattern of variations of the coefficient magnitude, corresponding to 7 s pulses, with a period of about 100 s. That period is clearly seen in the bottom of ampligram as an independent component with coefficient magnitudes less than 4%.

The summation along columns of the matrix  $Y$  should result in the original sample  $y(t_i)$ , if there would be no energy leakage from outside the filter band (7). Figure 7 shows results of summation (thick line) of seconds 700 – 800 of the ampligram in Fig. 5 together with the measured data (thin line). It may be seen that the differences between the observed and reconstructed data are of the order of 10%, which means that the energy leakage from outside the pass-band is not very important.

In order to investigate the presence of weak components in the signal the low-20 ampligram is a useful tool. The low-20 ampligram for the data shown in Fig. 5 is shown in Fig. 8. Another presentation method is used here. Since all horizontal cross-section of the ampligram are bipolar, the graphical presentation may be simpler if only positive (or negative) portion of the signal is plotted. Here

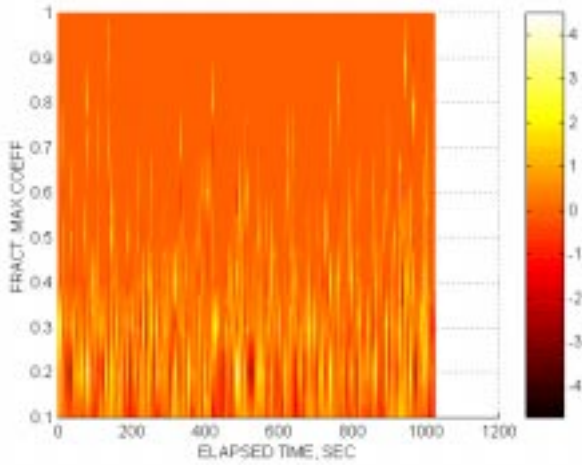


**Fig. 5.** A total ampligram of a 1024-point sample of photon counts with a frequency spectrum shown in Fig. 4. Sampling bin width is 1 s. The color scale is expressed in counts/second - zero corresponds to the average counts. Columns of the ampligram matrix are plotted in horizontal direction

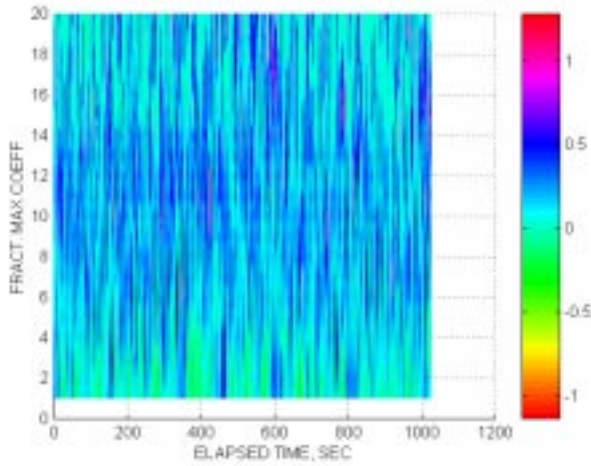


**Fig. 6.** A low-20 ampligram of the X-ray pulsar 1E2259+586, ROR 400314. Sampling bin width is 0.25 s

only positive portion of the ampligram is plotted for clarity. The color scale shows the natural logarithm of the amplitude  $y_l(t)$ . The use of logarithmic  $z$ -scale enhances the lowest amplitudes.

The ampligram demonstrate the amplitude and phase of components of the signal corresponding to different spectral densities. The ampligram is an useful method of presentation of the physical properties of the signal. The signal in Fig. 5 with highest coefficient magnitudes (40 – 100%) is burst-like and random. Regular structures seem to be dominant below 10% of highest coefficient magnitudes (see Fig. 8). It may be determined whether there is one or more semi-regular components in the signal. A

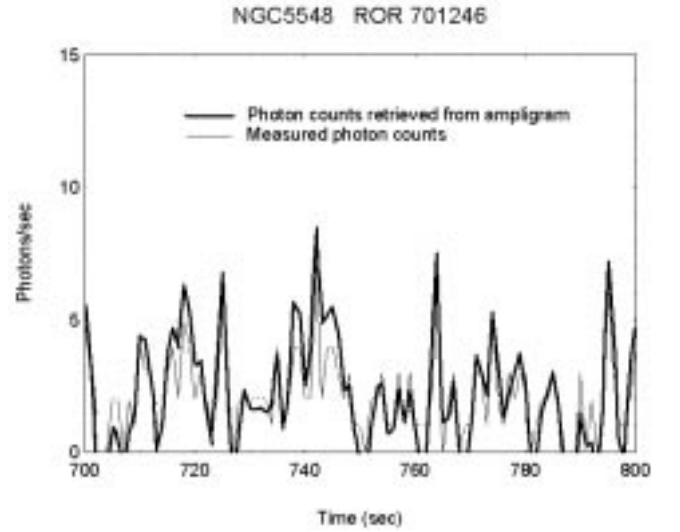


**Fig. 7.** Results of summation (thick line) of the first 5.5 s of ampligram in Fig. 5 together with the measured data (thin line)

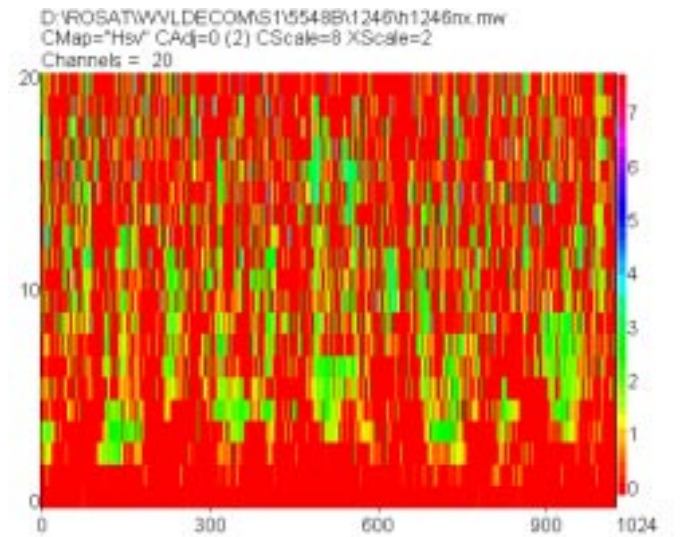


**Fig. 8.** The low-20 ampligram of the same data as shown in Fig. 5. Only positive portion of the ampligram is shown for clarity, logarithmic  $z$ -scale

decomposition technique for an ampligram is discussed in the following section.

## 5. Principal component analysis (PCA)

In the case of threshold filtering, described in Sect. 3, the kurtosis criterion is used to find the optimum threshold which must be set to separate the deterministic component from the stochastic one. In a general case, with several components, or with two deterministic components the kurtosis criterion may be difficult to use. In that case components may be separated by performing the principal

component analysis of the ampligram matrix. The principal component analysis is a method to resolve a data matrix into a number of orthogonal components. If the data matrix is a sample of a multivariate time series, the principal components, in which the matrix is resolved, reflect the independent, orthogonal constituents of the process described by the multivariate time series.

Since the ampligram may be considered as a multivariate time series ( $L = 20$ ,  $N = 1024$  for the above low-20 ampligram) the principal component analysis may be used to identify the number of independent modes in the data. A multivariate time series consisting of  $L$  variables measured at  $N$  equally separated instants forms a matrix  $Y$ . The next step of the analysis is to perform the principal component analysis (PCA) of the matrix  $Y$ . The results of PCA are:

- The vector of eigenvalues of the matrix (latent roots  $\lambda_l$ ), telling how much of the total variance in the matrix may be explained by the consecutive principal components;
- The matrix of component loadings, being correlation coefficients between old variables and the principal components (new variables);
- The matrix  $a$  of component score coefficients, a transformation matrix between the old system of  $M$  variables and the principal components (the new coordinate system);
- The matrix  $S$  of component scores, with one column for each principal component, being a projection of old  $M$  variables upon the new coordinate axis (directions of principal components).

The matrix  $S$  of component scores is thus the new multivariate time series in the principal component space. It has been found by the present author that, in all cases when filtering was performed in the principal component space, a considerable improvement of signal-to-noise ratio has been obtained without distorting the signal. Each column of  $S$  is low-pass filtered using a simple filter. The result of filtering is matrix  $S_f$ . After filtering an inverse transform:

$$Y_f = S_f \cdot a^{-1} \quad (8)$$

is performed resulting in a new version of the matrix  $Y$ . It is possible to combine the filtering procedure with a decomposition procedure. If one wants to know what the variations of the  $M$ -component vector would be with only one mechanism (or cause), corresponding to the principal component  $l$  active, it is possible to mask with zeros all other columns in  $S_f$ , except column  $l$  and to perform a calculation of a new matrix  $Y_{lf}$ :

$$Y_{lf} = S_f \cdot a^{-1}. \quad (9)$$

The operation may be repeated for each interesting component  $l$ . As the principal component transformation preserves the variance, the sum of all latent roots,  $\lambda_l$ , is equal

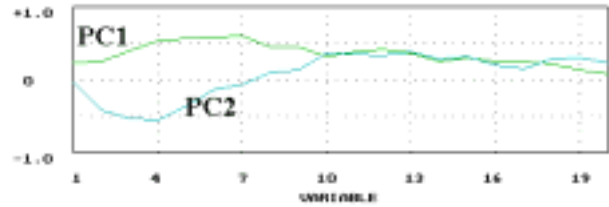


**Fig. 9.** Component loadings of the principal components PC1 & PC2 for the ampligram of Fig. 8. X-axis shows variable/wavelet coefficient magnitude in 1% steps of 20% of its maximum value

to the total variance. If the data is standardized, i.e. normalized to standard deviation for each variable, the sum of latent roots is equal to number of variables. The magnitude of latent roots is usually expressed in percent of the total variance. If the data contains only pure noise, all variables will be uncorrelated, and the total variance will be evenly distributed between all latent roots:

$$\lambda_l \text{ noise}(\%) = \frac{100\%}{L}. \quad (10)$$

The real data, measured or computer simulated, are never perfectly uncorrelated and the variance will not be evenly distributed between all latent roots. When all variables are related to the same common factor there will be one latent root (the first one, corresponding to the first principal component) significantly larger than the value indicated by (10).

## 6. Decomposition into independent modes

The principal component analysis of the ampligram matrix must be performed to identify the number of significant independent components in the data. As a result the matrix of component loadings, being the correlation coefficients between significant principal components of the ampligram and the  $L$  rows of the ampligram, is obtained. An example of component loadings is shown in Fig. 9. The diagram shows which ranges of coefficient magnitude between 0 and 20% contribute to the two modes present in the data of Fig. 8. The mode 1 (dominating) corresponds to coefficient magnitudes 4 – 10% and the mode 2 corresponds to magnitudes of 1 – 4%. The non-linear filtering is now repeated once for each observed mode, the bandpass of magnitude is now selected from Fig. 9. The result, after the inverse wavelet transform, shows time series corresponding to the significant modes. An example of decomposed modes is shown in Fig. 10.

## 7. Time scale spectrum of an ampligram

The ampligram may be used for calculation of average wavelet spectra, one for each coefficient magnitude. It is equivalent to performing, once again, the forward wavelet

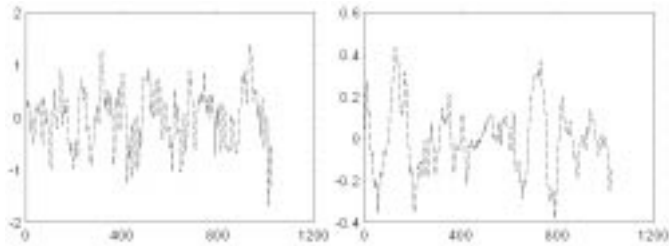


Fig. 10. Modes decomposed from the signal of Fig. 8

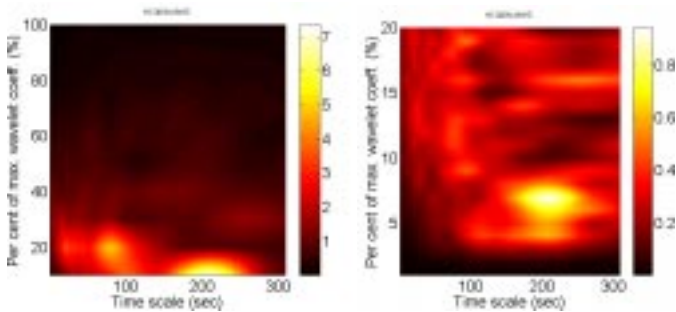


Fig. 11. Time scale spectra of the total ampligram (left) and of the low-20 ampligram (right) of the X-ray data from ROSAT, ROR 701246

transform on the filtered, inverse transformed data, that constitute the ampligram.

The procedure will generate a 3-D graph showing the time scale of the signal on the  $x$ -axis, the wavelet coefficient magnitude of the original signal, in percent of its max value, on the  $y$ -axis and the wavelet coefficient magnitude (corresponding to the power spectral density) of the decomposed component as the color scale. A graph of that kind will show the average properties of the different modes, if such exist, during the entire sample period.

The algorithm is as follows. Each row of the ampligram matrix,  $Y$ , is wavelet transformed, resulting in  $L$  matrices. We then time-average these matrices (average along rows) leading to  $L$  arrays,  $\bar{w}_l$ , with  $J$  elements. Construct an  $L \times J$  matrix,  $\bar{Y}$ , with  $\bar{w}_l$  as rows. This matrix  $\bar{Y}$  is the time scale spectrum of the ampligram.

Examples of time scale spectra of total ampligrams (left) and low-20 ampligrams (right) of the data ROR 701246 are shown in Fig. 11.

The interesting property of this graph is that deterministic periodic or semi-periodic structures in the data are mapped on the graph as vertically elongated features, while purely stochastic structures are mapped as horizontally elongated features. That property of the time scale spectrum may be illustrated as follows: A pure and stationary sine-like signal will be mapped on the time scale spectrum as a single dot. Introducing random phase variations, but without changing the signal amplitude will broaden the dot in the horizontal direction. On the other hand, introducing random amplitude fluctuations, with-

Table 1. Time scales present in time scale spectrum of 1E2259+586

No.	Explanation	Time(sec)	$\log(\text{Time})$
1	$T1$	4.17	0.620
2	$T$	6.98	0.844
3	$T + T2$	9.79	0.991
4	$T + T1$	11.14	1.047
5	$2 * T$	13.96	1.145

out scrambling the phase, will broaden the dot in the vertical direction.

For the X-ray pulsar ampligram of Fig. 6 the time scale spectrum may be useful to resolve different frequency components. Since the pulsar 1E2259+586 has a secondary maximum, located asymmetrically with respect to the middle of the period, it may be expected that the scalogram of the photon count series will be quite complex. According to Fig. 3 of Parmar et al. (1998) the secondary maximum is approximately 4.17 s ( $T1$ ) from the preceding main maximum and 2.81 s ( $T2$ ) from the following main maximum. With the pulse period  $T$  of approximately 6.98 s, time scales of Table 1 may be identified in time scale spectrum of ampligram of Fig. 6 shown in Fig. 12.

Positions of above components in the time scale spectrum are indicated by white lines, numbered as in Table 1. At least a part of information contained in the occurrence of those time scale components, together with their relative intensities may reflect the nature of the process responsible for the pulsar's emission.

## 8. Amplitude distributions of the ampligram and their entropy

A complementary information may be obtained from the ampligram constructing a set of amplitude distributions of  $y_l(t_i)$ , one for each level  $l$  of wavelet coefficient magnitude. For levels with pure stochastic component, Gaussian amplitude distributions will be obtained. For levels with deterministic components, broader amplitude distributions, often revealing structures, will be found. An example of distribution plot for ROSAT, ROR 701246 is shown in Fig. 13. In order to enhance sides of the distributions a logarithmic probability density scale is used. The amplitudes used to construct the graph in Fig. 13 are normalized to the maximum value of  $y_l(t_i)$  for each  $l$ . It may be seen that for wavelet coefficient magnitudes between 0.02 and 0.16 the distribution is broadened, which is in agreement with the part of ampligram where deterministic structures may be seen.

A useful method to quantify the above observation is to calculate the distribution entropy for each level of wavelet

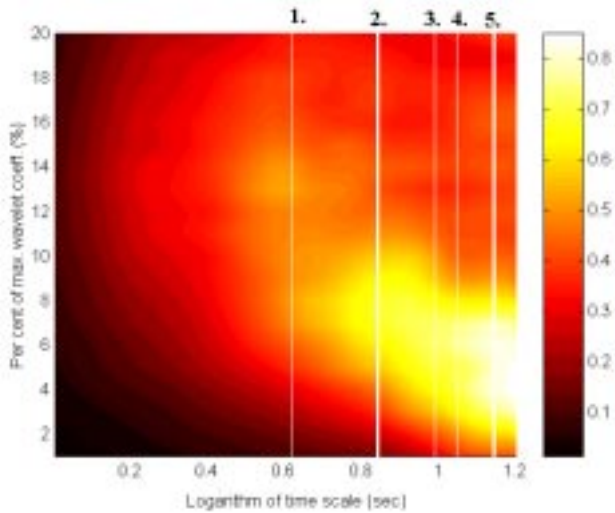


**Fig. 12.** Short time scale part ( $t < 16$  s) of the time scale spectrum of the X-ray pulsar 1E2259+586, ROR 400314. Vertical lines indicate position of different time scale components shown in Table 1. The logarithm of the time scale is displayed on the  $x$ -axis

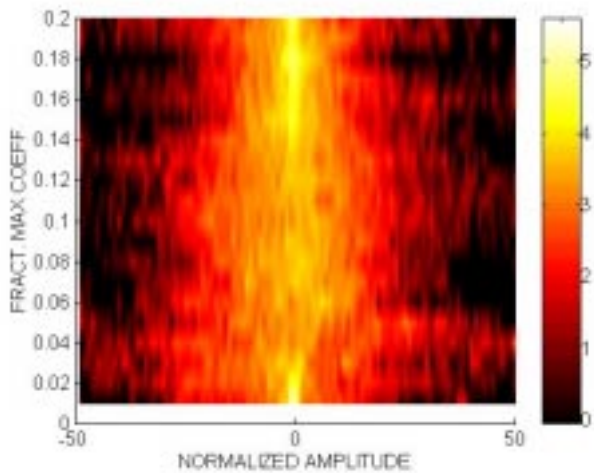


**Fig. 13.** An amplitude distribution graph for the ampligram in Fig. 8. (ROR 701246). The horizontal scale shows the normalized amplitude, vertical scale shows fraction of the maximum wavelet coefficient magnitude and the color scale shows the logarithm of the relative occurrence frequency

coefficient magnitude. The distribution entropy,  $E_l$ , is calculated as:

$$E_l = -\sum_i p_{il} \ln p_{il}, \quad i = 1, 2, \dots, B; \quad l = 1, 2, \dots, M \quad (11)$$

where  $p_{il}$  is the measured probability density,  $B$  is number of distribution bins (100 in our case), and  $L = 20$  for a low-20 ampligram. The entropy for the amplitude distribution pictured in Fig. 13 is shown in Fig. 14. It may be seen that the broadened distribution corresponds to an increase of entropy. However, it must be remembered

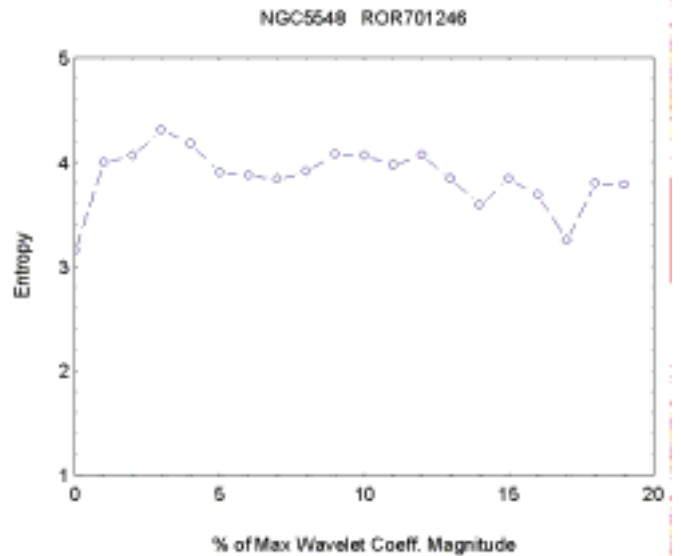


**Fig. 14.** The distribution entropy as a function of the fraction of the maximum wavelet coefficient magnitude for the distribution graph of Fig. 13

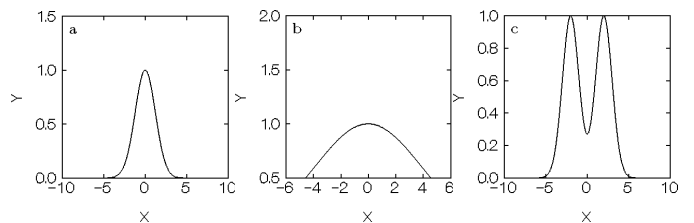


**Fig. 15.** The distribution shape and the value of entropy: **a)** pure Gaussian noise, narrow distribution, low entropy; **b)** the distribution broadened due to presence of semi-regular components with different periods, increased entropy; **c)** strong harmonic component in the data, decreased entropy

that distinct multiple peaks, if such appear in the distribution, will again decrease the entropy. That is illustrated in Fig. 15.

The distribution entropy will be used in the present study as a measure of occurrence of deterministic structures.

## 9. Sensitivity of the ampligram method

An interesting problem is the sensitivity of the method; i.e. what is the smallest amplitude of the deterministic component which may be detected when immersed in a pure Poisson-like background. A detailed study using different types of deterministic components was performed. The results will be published elsewhere, here only a short summary of relevant results will be given. The Poisson-like background was generated using the beta-decay event series. It is assumed in physics that the radioactive decay is a classical Poisson process. In the present study beta-decay pulses were counted in a series of 1 s bins. The radioactive

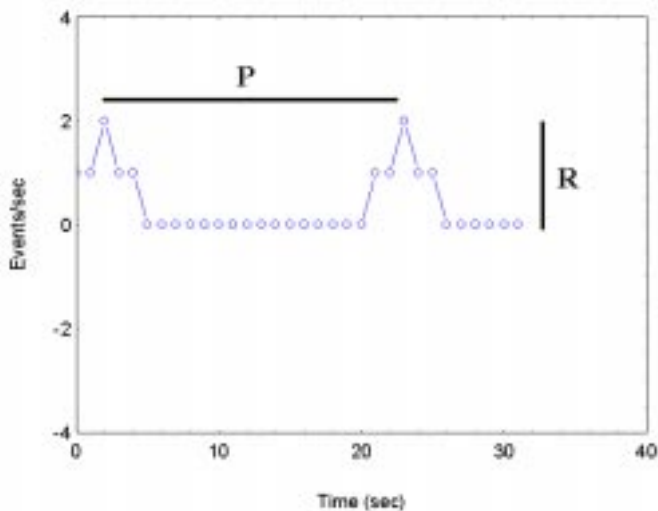


**Fig. 16.** Deterministic component added to beta-decay series. In the present example  $P = 57$  bins and  $R = 3$  events/bin

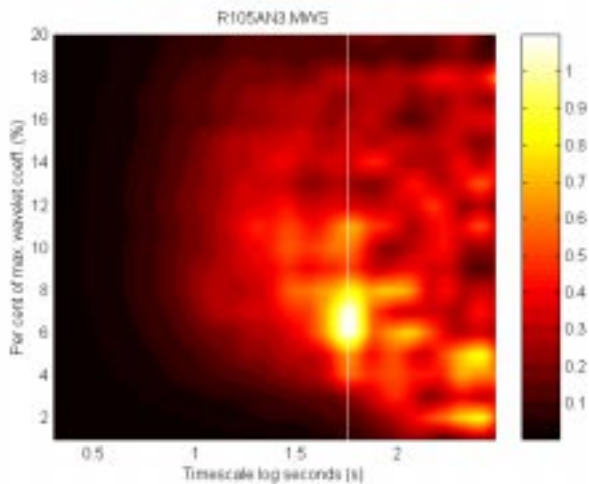


**Fig. 17.** Time scale spectrum of beta-decay data with a superimposed deterministic component shown in Fig. 16. The white vertical line indicates the period of the deterministic component

source was collimated so that the average counting rate during the entire 1024 s sample was around 1 event/s. The deterministic component used in the present example was of the type shown in Fig. 16, with a period  $P$  bins and a maximum amplitude  $R$  counts/bin.

The ampligram and time scale spectrum was calculated for the synthesized series. The time scale spectrum is shown in Fig. 17. A logarithmic scale is used on the horizontal axis of time scales. The white line on the diagram indicates the period of the deterministic component,  $P = 57$  s.

In the demonstrated case the deterministic component contains about 15% of photons in the background. It has been found that for average counting rate of 1 event/s a deterministic component containing 8% of background

photons may still be detected on the time scale spectrum. The sensitivity of the method seems to be dependent on the average counting rate. Transferring this result to continuous signals it would correspond to detection of a signal 22 dB below the background level.

## 10. Analysis of simulated photon flux

In the case of X-rays from AGN there might be a physical source of deterministic variations of the photon flux. Pacholczyk & Stoeger (1994) propose “building blocks” in the X-ray photon flux from active galactic nuclei. In the present study each building block is assumed to be formed by a Poisson process. A Poisson process may be simulated (Råde & Westergren 1995) using a series of random numbers according to the formula

$$t_i = t_{i-1} - \frac{\ln X_{ni}}{C} \quad (12)$$

where  $t_i$  is time of event  $i$ ,  $X_{ni}$  is a random number between 0 and 1 and  $C$  is the Poisson parameter, called also the process intensity. The event series is then converted into an event rate plot by counting events in consecutive time bins. In the present case it is assumed that each block is a fragment of a Poisson process with the process intensity within each block,  $C$  decreasing with time according to:

$$C = C_0 t_j^{-k} \quad (13)$$

where  $C_0$  is the starting process intensity,  $t_j$  is the time of the  $j$ -th photon measured from the beginning of the building block and  $k$  is the exponent determining the rate of decay of the block. The simulations were performed assuming random values for the number of photons in each block, NP, the number of building blocks during the simulation period, NB, and a pair of values for  $C_0$  and  $k$ . The results of simulations have shown that there will be a significant difference in the character of time scale spectrum depending on if building blocks are superimposed in a semi-regular manner or randomly. Figure 18 (left diagram) shows the time scale spectrum for randomly superimposed blocks (NB = 35, NP = 214,  $C_0 = 12.6$  and  $k = 2.27$ ), while in the right diagram the building blocks were superimposed in a semi-regular manner (NB = 8, NP = 238,  $C_0 = 5.0$ ,  $k = 0.615$  and the average period between blocks is  $200 \pm 40$  s). Note the linear scale of  $x$ -axis on both diagrams.

It may be seen that the character of superposition of Poisson-like building blocks may be studied using the present method. Also number of building blocks per time unit may be determined.

## 11. Conclusions

The ampligram may be considered as an analogy to signal decomposition into Fourier components. In that case

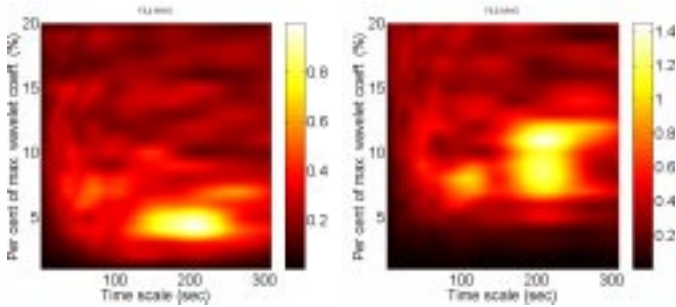


**Fig. 18.** Time scale spectrum of simulated superposition of building blocks: random (left) and semi-regular (average period  $200 \pm 40$  s) (right diagram). Linear scale of  $x$ -axis

different components correspond to different frequencies. In the present case different components correspond to different wavelet coefficient magnitudes, being equivalent to spectral densities. A useful property of the ampligram is that when integrated along the coefficient magnitude axis, the original signal should be obtained. However, if the original signal spans over a large range of amplitudes, the energy leakage into the ampligram band will occur and the integral of the ampligram will show values larger than those of the original signal.

The time scale spectrum of the ampligram tells us more than the original wavelet spectrum does. The time scale spectrum reveals individual signal components and indicates the statistical properties of each component: deterministic or stochastic. The ampligram and its time scale spectrum seems to be a useful tool to study processes resulting in a mixture of stochastic and deterministic components. The most important point of the method is that it may be used to remove the influence of the Poisson statistics in the photon data and in this way to extract real deterministic luminosity variations. As it is shown by simulations in Sects. 9 and 10 of this work, the method is capable to extract weak, deterministic variations embedded in a totally Poisson-like series of events. The entropy of amplitude distributions at the individual levels of wavelet coefficient magnitude was found to be a useful measure of the occurrence of deterministic components in an ampligram. In the case of X-ray luminosity variations in the AGN it is expected that the described data analysis technique will provide a conclusive proof of the existence of building blocks. The efficient decomposition of the luminosity variation data may be used to study the deterministic, quasi-periodic phenomena, like tones and chirps.

*Acknowledgements.* The authors are indebted to A.W. Wernik of Space Research Center, Warsaw, Poland, for support in the area of non-linear filtering using wavelets and to A.G. Pacholczyk and W.R. Stoeger of Steward Observatory, University of Arizona for continuing discussions in the course of this work and for support in matters concerning the AGNs. The software used in this work has been developed by Pär-Ola Nilsson, Jan Karlsson and Fredrik Rutqvist of the Umeå Division of the Swedish Institute of Space Physics. The data used to demonstrate the present analysis technique are ROSAT PSPC photon event history files obtained through the High Energy Astrophysics Science Archive Research Center Online Service, provided by the NASA/Goddard Space Flight Center.

## References

- Chui C.K., Montefusco L., Puccio L., 1994, *Wavelets: Theory, Algorithms and Applications*. Academic Press, Boston
- Daubechies I., 1992, *Ten Lectures on Wavelets*, SIAM, Philadelphia
- De Vries M., Kuijpers J., 1992, *A&A* 266, 77
- Farge M., 1992, *Ann. Rev. Fluid. Mech.* 24, 395
- Farge M., Philipovitch T., 1993, *Coherent structure analysis and extraction using wavelets*, in *Progress in Wavelet Analysis and Applications*. Éditions Frontières, Gif-sur-Yvette
- Lagoutte D., Cerisier J.C., Plagnaud J.L., Villain J.P., Forget B., 1992, *J. Atm. Terr. Phys.* 54, 1283
- Liszka L., 1996, *Reconstruction of Equidistant Time Series Using Neural Networks*, Technical report, Swedish Institute of Space Physics, <http://www.irf.se/ume/pdf/235rep.pdf>
- Pacholczyk A.G., Stoeger W.R., 1994, *AJ* 434, 435
- Parmar A.N., Oosterbroek T., Favata F., et al., 1998, *A&A* 330, 175
- Råde L., Westergren B., 1995, *Mathematics Handbook*, Studentlitteratur, Lund, p. 424
- Wernik A.W., Grzesiak M., 1997, in Sadowski M. and Rothkaehl H. (eds.), *Proc. Int. Symp. "Plasma 97"*, Jarnoltowek, Space Research Center, Polish Academy of Sciences, Vol. 1, p. 391